Journal of Engineering Science and Technology
Vol. 2, No. 2 (2007) 177 - 187

THE CFD APPROACH FOR SHEAR ANALYSIS OF MIXING REACTOR: VERIFICATION AND EXAMPLES OF USE

S. VLAEV[1]*, D. GEORGIEV[1], I. NIKOV[2], M. ELQOTBI[2]

[1]Institute of Chemical Engineering, Bulgarian Academy of Sciences,
Acad. G. Bonchev Str. Bl. 103, 1113 Sofia, BULGARIA.

[2]Polytech'Lille, Département IAAL ProBioGem, Université des Sciences et Technologies de Lille, Cité Scientifique, Avenue Paul Langevin, 59655 Villeneuve d'Ascq, FRANCE.
*Corresponding Author: mixreac@bas.bg

Abstract

The paper presents experimental evidence for the potentials of CFD methodology in revealing external flow and inner flow shear deformation rates in stirred tanks. Two basic issues are considered: could CFD produce valid solutions for shear rates in mixing vessels, and could practical shear rate differences relevant to specific impeller designs be reproduced by CFD. In a first part, the shear rate distribution in the flow fields of two basic impellers comprising flat and fluid-foil blades have been simulated and compared with measurement data obtained by electro-diffusion. Based on these and other reference data, coincidence of measured and simulation shear rates has been found. In a second part, a CFD shear deformation analysis procedure has been introduced and validated and shear rate functions relevant to two applications in viscous flow have been generated. The procedure is illustrated by practical examples showing its versatility for prompt characterisation of impeller shear deformation performance. Straight forward impeller selection by using CFD is implied.

Keywords: Mixing, Shear Rate, CFD, Verification.

1. Introduction

Shearing forces in stirred reactors are responsible for producing fluid intermixing and homogenisation. Other important properties in multiphase applications

Nomenclatures

C_o	Bulk concentration of the ions (mol.m^{-3})
D	Impeller diameter (m)
D_{eff}	Diffusion coefficient of the active ions in the solution (m^2.s^{-1})
d_e	Circular microelectrode diameter (m)
F	Faraday constant
H	Liquid height (m)
I	Local diffusion limiting current
K	Consistency coefficient (Pa.s^n)
N	Impeller speed (rps)
n	Flow index (dimensionless)
n_z	Number of exchanged electrons
Re	Reynolds number in power law fluid mixing, $\rho N^{2-n} D^2 / K k_s^{n-1}$
$\dot{S}$	shear strain rate s^{-1}
T	Tank diameter (m)
V_i	Velocity component in the i-th direction (m.s^{-1})

Greek Symbols

ρ	Fluid density (kg.m^{-3})
τ	Shear stress Pa
μ	Fluid dynamic viscosity Pa.s
μ_a	Apparent viscosity, $\mu_a = K\dot{s}^{n-1}$ (Pa.s)
v_t	Turbulent viscosity (m^2.s^{-1})

Subscripts

a	Apparent
t	Turbulent

comprise bubbles and drops break-up and dispersion. The shear rate defined by velocity gradients is a major component estimate of this behaviour. A mixing impeller of general use may operate at various regimes depending on viscosity and could exhibit different shear fields depending on the flow geometry. The engineering response to practical requirements would depend on the shear analysis and the shear performance of impeller designs.

In a recent lecture, we have discussed impeller selection based on shear rate experimental measurement by the electro-diffusion technique [1]. The study delivered data for various impellers, liquids and regimes that could be used for validation of a CFD - facilitated shear deformation analysis in mixing vessels. Problems arose that were considered once by the authors in [2]. In what follows we have discussed two basic issues: (1) Can CFD produce valid solutions for shear rate in mixing vessels? and (2) Can practical shear rate differences relevant to specific impeller designs be reproduced by computational flow simulations? Were the answer 'yes', design selection based on CFD shear analysis could be put forward.

The importance of the problem is manifested by reference to recent papers in the literature. Examples are the studies regarding shear rates in non-baffled vessels and shear-thinning fluids [3, 4], maximum shear rates at flat blades and discs [5, 6], near-impeller shear rates of A315, A200 in power law liquids [7], shear at close-clearance impellers [8], shear rates by impeller-driven and oscillatory mixing [9], and wall shear rates in rotating surface heat exchangers [10].

2. Materials and Methods

In order to respond to the validation requirement of the study, both mathematical and real experiments of shear rate were performed or referred to.

2.1 The model

Since the study operated with time-average values of all variables, the velocity gradients could be generated by RANS. Consequently, at turbulent transition a RANS model was formulated. The model followed largely a known set of assumptions and a known set of equations already reported in previous analyses [11, 12]. Thus, it is not considered here in detail. For the turbulent mixing regime, the standard *"k-ε"* approximation was used. The general Navier-Stokes model was solved at laminar flow conditions, Re<100. The solution model was based on the 'inner-outer reference frames' approach [13]. The flat blade walls and the walls of a spherical particle/probe ware meshed by grid refinement with up to 800 000 cells using Gambit 1.2. The representative data were volume and surface integral averaged shear rate values, depending on their relevance as 'fluids' or 'walls', respectively. General validation by power numbers and mixing time, as well as by LDA has been completed previously [12, 14, 15].

2.2 Definition of strain rate

Regarding the viscous shear, the modulus of the rate of strain tensor was used as a characteristic value for the shear rate [6].

$$\dot{S}_{ij}=\left(\frac{\partial V_i}{\partial x_j}+\frac{\partial V_j}{\partial x_i}\right) \tag{1}$$

Focusing on turbulent transitional flow, the average velocity gradient $\dot{s}_{ij}$ of the dominant component stress, $\tau_{ij}=-\rho\nu_t\dot{s}_{ij}$, that represents friction was determined. Mostly laminar and transitional flow conditions were considered where shear stress *ij* components prevailed and the standard feature of Fluent could be used. In order to balance the prevailing components in the multiple directions and thus to characterize the average velocity gradient specific for the analysis reference position, the gradients $\dot{s}_{ij}$, were determined as an average value among the values obtained at different angles to the main flow. Both external and inner flow gradients $\dot{s}$ were examined.

2.3 Physical experiment

A contact measurement scheme has been selected for the analysis. The electro-diffusion measurement method [16] using a mobile spherical probe immersed in the liquid (Fig. 1) was used. The local diffusion limiting current resulting from fast reduction of ferric cyanide ions over the probe boundary, I_d, was measured. The near-probe wall shear rate $\dot{s}$ was related to I_d by the equations:

$$\dot{s} = \left(\frac{1.477}{n_z F}\right)^3 \cdot \frac{I_d^{\,3}}{D_{eff}^{\,2} C_0^2 d_e^5} \tag{2}$$

As D_{eff} the molecular diffusivity of ferric ions in the solution, 6.7 $\cdot 10^{-10}$ m^2/s [16] was used, C_0 was 2 $mol.m^{-3}$.

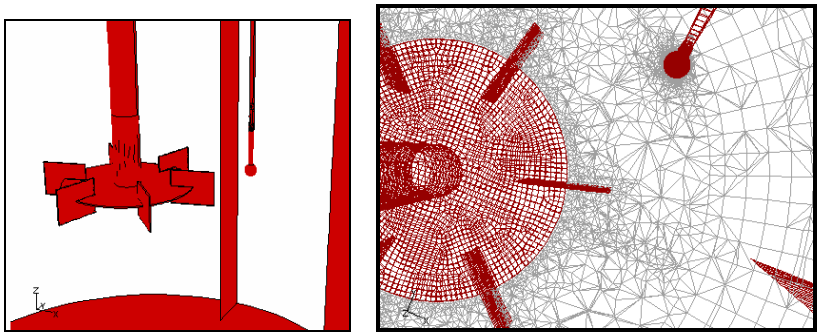

Fig. 1. Experimental Set-Up for Measurement of Shear and Extended Mesh Refinement for its Simulation.

Practically, the polarographic probe was immersed in different fluids and in different zones of the stirred vessel in Fig.1. The ionic electro-diffusion rate in the boundary layer around the spherical probe was measured and interrelated with the shear rate obtained according to Eq. (2) [16]. Additional shear rate data were delivered from the literature [6, 18, 19].

Other experimental details included the mixing vessel with the impeller being centrally located. In order to keep up with the reference measurement conditions, standard configuration of $D=T/3$ was assumed; the liquid height was $H=2D$, and the tank diameter $T=0.4$m. The spherical probe was 10 mm in diameter and it contained the circular microelectrode of 1 mm diameter. Further details will be subject to the presentation.

3. Results and Discussion

3.1 Validation of the numerical procedure to generate shear rates

The physical experiment was simulated by computational flow modelling and the model was solved by FLUENT v.6.1 [17]. Referring to the case of Rushton turbine in the vessel, the validation runs at N=600 rpm produced the results presented in Table 1. Considering the reference measurement methods, Van't Riet and Smith [18] and Metzner and Taylor [19] have used high-speed photography, and Wichterle et al. [5] have used polarography.

Table 1. Experimental vs. Predicted Shear Rates Generated by Rushton Turbines.

No	Parameter	$\dot{S}$ /N measured	$\dot{S}$ /N predicted by CFD [this study]
	Shear rate on impeller blades	Acc. to [5]:	
1	Flat blade av. values in water $Re>10^4$	600-1200	660 (Re $1.1.10^4$)
	Near-particle average shear rate	[this study]:	
2	in water	910-1000	600-1500
3	in power law CMC 30 mPa.s (n=0.75, K=0.1 Pa·s^n)	600-800	300-800
4	in power law XG 14 mPa.s (n=0.38, K=0.26 Pa·s^n)	550-900	300-900
	Vortex-average inner flow velocity gradient	Acc. to [18]:	
5	at Re > 10^4	40-90	20-86
6	at Re > 5.10^3	20-60	24-55
	Shear rate in the flow of baffled tanks	Acc. to [19]:	(see also Fig. 3)
7	Impeller area in Karo Syrup 2 Pa: at 2r/T=0.33	20-40	40-70
8	at 2r/T=0.5	3-4	<10

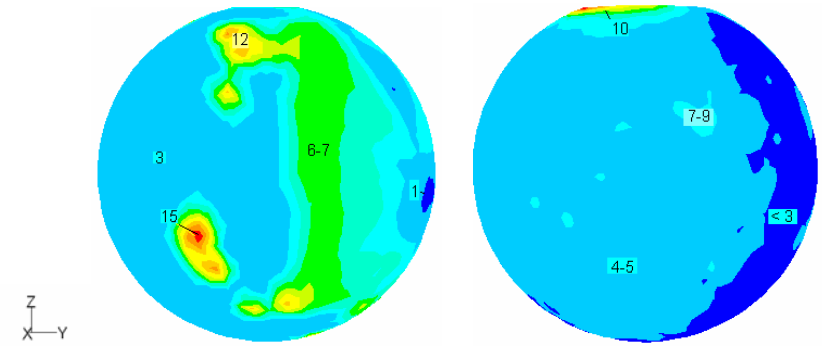

a **b**

Fig. 2. Simulation Set-Up and CFD Strain Rate Contours (in ks^{-1}) Obtained at the Spherical Particle Wall by RT mixing at N=10 rps in Cases of Water (a) and power law liquid (K=0.38 Pa·s^n, n=0.26) (b) μ_a=12 mPa.s.

A 2D visualisation of the validation experiment with a spherical probe is illustrated in Fig. 2. The reality $\dot{s}$ - figures measured by the electro-diffusion technique in similar probe positions, i.e. in the impeller plane at the point 2 cm off the impeller tip and at N=10 rps, were $\dot{s}$ ~10 ks^{-1} (a) and $\dot{s}$ ~6.6 ks^{-1}(b). These data correspond to cases 2 and 4 in Table 1.

Consequently, the CFD prediction of the local shear rate in stirred vessels is comparable with the measurement results. With significance to impeller characterization, the fact implies that one may use successfully CFD-generated $\dot{s}$ -values in place of measurement results.

3.2 Using the numerical procedure to generate functions of shear rate

The CFD under the FLUENT code was used further to determine the shear fields and to study the differences of the shear characteristics relevant to different impeller designs and to the stirred liquids. These functions have been examined in order to estimate the potential of the CFD methodology.

The following functions were considered:

1. Shear rate vs. dynamic viscosity in laminar flow.
2. Shear rate vs. power effective viscosity in power law fluids at transitional flow.

In order to justify impeller selection by CFD, two impellers of different type were computer-rendered, e.g. a flat-blade turbine (indicated as Rushton RT) and a fluid foil impeller termed Narcissus (NS) [14].
The Newtonian liquids were represented by dynamic viscosity. Power law fluids were mimicked by effective viscosity and by introducing the relevant power law constants. Detailed data has been presented in [20].

3.2.1 Matching the Metzner-Otto relationships in laminar flow

As determined by the impellers' Metzner and Otto constants k_s [6, 20], the ratio of the experimental average shear rates at identical rpm should be $k_{s\,(RT)} / k_{s\,(NS)} \approx$ 11.5 / 8.1. Thus, also the ratio of average shear rate obtained for RT and NS by simulation at similar flow conditions should vary proportionally to ca. 1.4.

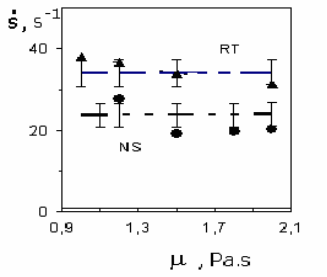

Fig. 3. CFD Generated Relationships Of Volume-Averaged Shear Rates Vs. Dynamic Viscosity In Laminar Flow.

Matching the experimental conditions, the CFD average shear rates were determined. Volume-weighted average $\dot{s}$ -values valid for Newtonian viscous flow are plotted vs. dynamic viscosity in Fig. 3. Evidently, the predictions of average shear rate with $\dot{s}$ =34s^{-1} corresponding to RT and $\dot{s}$ =24s^{-1} corresponding to NS met the expected condition of $k_{s\ (RT)}/k_{s\ (NS)} \approx 1.4$ within the 10 % constancy tolerance illustrated.

3.2.2 Study of impeller flow field deformation capacity in power law flow

Again impeller RT and impeller NS have been compared. The following procedure was followed:

1. The measurement probe positions were selected to correspond to the maximum discharge paths of the impellers - as shown in Fig. 4.

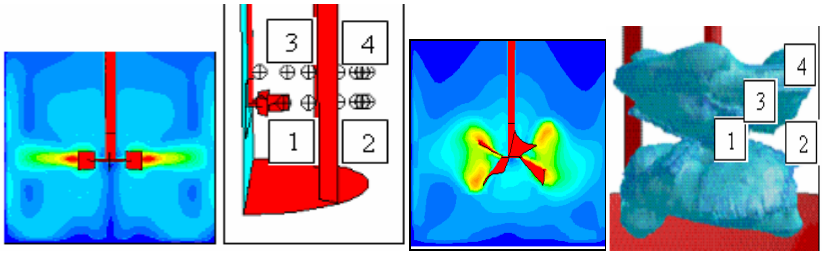

Fig. 4. Selected Positions Observed by CFD Simulation and In The Experiments

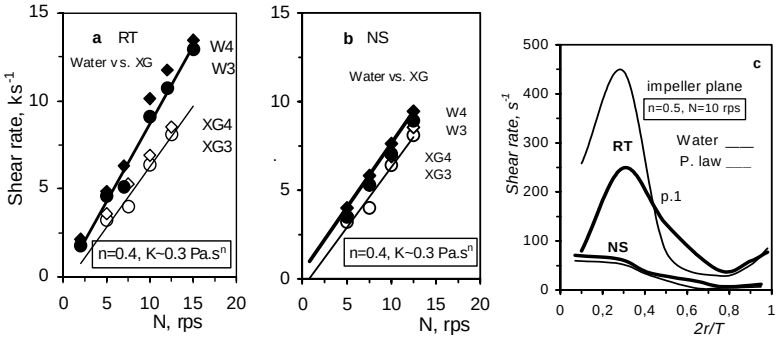

Fig. 5. Selective Shear Rate (In Ks^{-1}) Damping In Power Law Flow Affected By Impeller Design: Experimental Near-Particle $\dot{s}$ (a) (b) and CFD-Inner Flow $\dot{s}$ Profiles (c) Corresponding To RT And NS: A Qualitative Comparison.

2. The shear rates $\dot{s}$ in various liquids at these points were measured. Example data of $\dot{s}$ in xanthan gum and water are plotted vs. impeller speed N in Fig. 5. The relationships obtained in positions 3, 4 of Fig. 4 are illustrated. Additional data has been reported elsewhere [16].
3. The separate cases were simulated and post-processed by CFD and the results were analyzed. The reduction of shear rate in polymer presence corresponding to cases RT and NS in Fig. 5 is summarized in Table 2. Example shear rate iso-surfaces' areas simulated for the impellers in laminar flow, e.g. μ=2 Pa, showed similar drag reduction trends (Fig.6). The data documented in presence of polymer additives showed what was expected from the flow field presentation of both impellers and what conformed to the experimental measurement data, i.e. a sharp reduction of shear in the stirred flow field produced by the flat-blade impeller and a moderate shear change generated by the fluid-foil NS. As illustrated in Fig. 6, at high viscosity both effects lead to comparable shear rate performance.

One could infer that the CFD shear analysis conforms to the physical reality of drag reduction in non-Newtonian flow, the degrees of drag reduction being described qualitatively.

The following outcome of the study is foreseen: The physical experiment could be replaced by CFD characterization that could lead to a prompt impeller selection

Table 2. Selective Impeller Shear Rate Damping in Power Law Flow Apart From the Impeller.

Simulation of shear rate in p.3 *produced the following*	*data*
RT : $\dot{S}$ =9.7 s^{-1}, in water changes strongly into $\dot{S}$ =6.6 s^{-1} in power law fluid	NS: $\dot{S}$ =3.6 s^{-1}in water changes slightly into $\dot{S}$ =4.3 s^{-1} in power law fluid
Simulation of shear rate in p.1 *produced the following*	*data corresponding to Fig. 5c*
RT: $\dot{S}$ =134 s^{-1} in water changes strongly into $\dot{S}$ = 78.5 s^{-1} in power law fluid	NS: $\dot{S}$ =35.3s^{-1}in water changes slightly into $\dot{S}$ =30,7s^{-1} in power law fluid
*Further numerous examples can be produced.	**Coordinates of P.1 (2r/T=0.5, z/H=0.5) P.3 (2r/T=0.5, z/H=0.6)

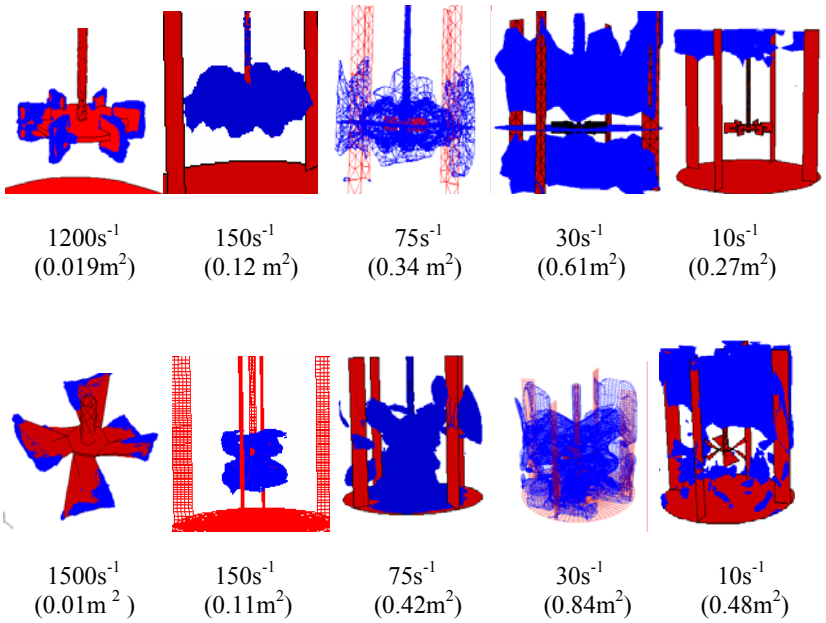

Fig. 6. Iso-Zones Corresponding to Different Strain Levels At Viscosity 2Pa; Re=100. (The surface area indicated in brackets represents the relevant strain rate spatial distribution).

4. Conclusions

The CFD approach for prediction of the deformation potential of different impeller designs in stirred reactor shear analysis is introduced on the basis of physical evidence. The shear rate distribution of the flow fields of two basic impellers comprising flat and fluid-foil blades is simulated and compared with experimental data from electro-diffusion measurements. Based on these data, the simulation shear deformation analysis is validated. The procedure is illustrated by practical visualization examples showing its versatility for fast qualitative characterization of impeller performance. Straightforward impeller selection by using CFD has been implied.

References

1. Vlaev, S.D., Nikov, I. & Martinov, M. (2004). Velocity gradients in impeller-agitated power law liquids at transitional mixing, *Paper at ISMIP5*, Sevilla, 1-4 June.
2. Vlaev, S.D., Georgiev, D., Nikov, I. & Elqotbi, M. (2006). Shear analysis of mixing reactors – verification of the CFD approach. *Proceedings of the 12th European Conference on Mixing* (Editors: F.Magelli, G.Baldi, A.Brucato), Bologna (Italy), 479-486.

3. Kaminoyama, M., Saito, F. & Kamiwano, M. (1990). Flow analogy of pseudoplastic liquid in geometrically similar stirred vessels based on numerical analysis. *J. Chem. Eng*. (Japan), **23**, 214-221.
4. Sanchez Perez, J.A., Rodriguez Porcel, E.M., Casas Lopez, J.L., Fernandez Sevilla, J.M. & Chisti, Y. (2006). Shear rate in stirred tank and bubble column reactors. *Chem. Eng. J.* 124, 1-5.
5. Wichterle, K., Kadlec, M., Zak, L.& Mitschka, P. (1984). Shear rates on turbine impeller blades. *Chem. Eng. Commun*., **26,** 25-32.
6. Paul, E., Atiemo-Obeng, V. & Kresta, S. (Eds.) (2004). *Handbook of industrial mixing science and practice*. New Jersey: Wiley.
7. Kelly, W. & Gigas, B. (2003). Using CFD to predict the behavior of power law fluids near axial flow impellers operating in the transitional flow regime. *Chem. Eng. Sci*., **58**, 2141-2152.
8. Murthy Shekhar, S. & Jayanti, S. (2003). Mixing of power-law fluids using anchors, *A.I.Ch.E.Journal,* **1**, 30-40.
9. Chew, C.M., Ristic, R.I., Reynolds, G.K. & Ooi, R.C. (2004). Characterization of impeller driven and oscillatory mixing by spatial and temporal shear rate distributions. *Chem. Eng. Sci*., **59**, 1557-1568.
10. Mabit, J., Fayolle, F. & Legrand, J. (2003). Shear rates investigation in a scraped surface heat exchanger. *Chem.Eng. Sci.,* **58**, 4667-4679.
11. Vlaev, S.D., Staykov, P. & Kraitschev, S. (2003). Numerical analysis of the drag-reducing performance of blade shape in stirred power law fluids. *Preprints of the 11th European Conference on Mixing,* Bamberg, VDI-GVC, Dusseldorf, 331-338.
12. Vlaev, S.D., Staykov, P. & Popov, P. (2004). Pressure distribution at impeller blades of some radial flow impellers in saccharose and xanthan gum solutions: a CFD visualization approach. *Trans. IChemE*, **82** (C1), 13-20.
13. Brucato, A., Ciofalo, M., Grisafi, F. & Micale, G. (1998). Numerical prediction of flow fields in baffled stirred vessels: A comparison of alternative modeling approaches. *Chem. Eng. Sci.* **53** (21), 3653-3684.
14. Vlaev, S.D., Mavros, P., Seichter, P. & Mann, R. (2002). Operational characteristics of a new energy-saving impeller for gas-liquid mixing. *Can. J. Chem. Eng.*, **80**, 653-659.
15. Mavros, P., Mann, R., Vlaev, S.D. & Bertrand, J. (2001). Experimental visualization and CFD simulation of flow patterns induced by a novel energy-saving dual configuration impeller in stirred vessels. *Trans. IChemE* 79A, 857-866
16. Vlaev, S.D., Nikov, I. & Martinov, M. (2006). Shear and skin friction on particles in power-law fluids agitated by flat-blade and fluid foil impellers. *Chem. Eng. Sci.* , **61** , 5455-5467.
17. Fluent Inc. (2003). *Fluent 6.1 Documentation*. CD, New Hampshire.
18. Van't Riet, K. & Smith, J.M. (1975). The trailing vortex system produced by Rushton turbine agitators. *Chem.Eng. Sci.,* **30**, 1093-1105.
19. Metzner A.B. & Taylor, J.S. (1960). Flow patterns in agitated vessels. *A.I.Ch.E. J.*, **6**, 109-114.

20. Martinov, M. & Vlaev, S.D. (1999). Average shear rate and power consumption of a curved-blade impeller for shear-thinning fluids. *Bulg. Chem. Commun*., **31**, 471-76.